ILASS 2008
Sep. 8-10, 2008, Como Lake, Italy

Paper ID ILASS08-4-2

# HEAT AND MASS TRANSFERS OF EVAPORATING DROPLETS USING OPTICAL TECHNIQUES: INFLUENCE OF THE FUEL

V. Deprédurand*, G. Castanet*, F. Lemoine*

*Nancy-Université, LEMTA-CNRS UMR 7563
2, Avenue de la forêt de Haye, BP 160
54504 Vandoeuvre-lès-Nancy, France

**ABSTRACT**

The prediction of heat and mass transfers in fuel sprays is a key issue in the design of combustion chambers where the fuel is injected on a liquid form. The development and validation of new physical models requires reliable experimental data. This paper reports on an experimental study to characterize the Nusselt and Sherwood numbers of monodisperse droplets evaporating into flowing hot air. Simultaneous measurements of the droplet size and mean temperature evolution allowed evaluating the heat fluxes that take part in the evaporation process. The evaporation flux is characterized by the measurement of the droplet size reduction from the droplet laser light scattering in the forward direction, while the droplet mean temperature, required for the internal and convective heat flux evaluation, is determined by two-color, laser-induced fluorescence. The experimental Nusselt and Sherwood numbers are then compared to the case of an isolated droplet in order to highlight the effect of droplet-to-droplet interactions. The emphasize is then placed on the effect of the fuel nature. To that end, the measurements have been performed on several fuels (acetone, ethanol, 3-pentanone, n-heptane, n-decane, n-dodecane) that have very different volatilities. It appears that the Nusselt and Sherwood numbers are particularly reduced by the interactions in a way that depends on the fuel nature.

## INTRODUCTION

The evaporation of fuel sprays in combustion engines is well-known to have a strong influence on the pollutant emissions, ignition delays and overall combustor efficiency. When a fuel droplet enters into a high temperature environment like in a combustion chamber, the droplet is heated, evaporates and finally the fuel vapour burns, delivering the energy for propulsion. A reliable description of the heat and mass transfers in sprays is required to optimize the combustion chambers of the engines and make them fulfil environmental conditions in term of pollutant emissions. In a spray, the droplet dispersion is usually characterized by the Stokes number. When the Stokes number is of the order of unity, droplet clusters can be formed by vortex stretching and folding. In such clusters, heat and mass transfers are significantly reduced compared to an isolated droplet. If evaporation and combustion models for isolated, stagnant or moving fuel droplets are now widely available in the literature ([1-4]), the understanding of droplet-to-droplet interactions is still limited.

Studies dealing with this topic were generally based on numerical approaches and focalized on basic situations. Labowsky [5] and Marberry et al. [6] used the point sources method to determine the burning rates of stagnant droplets in finite arrays containing up to eight symmetrically arranged monodisperse droplets. Particle interactions were shown to be a function of particle size, number density and geometry of the array. Correction factors from which multiple particle burning rates can be calculated from single particle burning rates were established. Chiang and Sirignano [7,8] were able to take into account the effect of the droplet motion by performing a comprehensive numerical study of two and three evaporating droplets moving together. Their computation included: the effects of variable thermophysical properties, transient heating and internal circulation in the liquid phase, boundary-layer blowing, moving interface due to surface regression, and the relative motion between the droplets. They underlined the effect of the droplet spacing and the subsequent modifications of the Nusselt and Sherwood numbers. Imaoka and Sirignano [9-10] considered the vaporization of three dimensional droplet arrays. Burning rates were computed and correlated with the number of droplets, average droplet size, and average spacing for the array through one similarity parameter for arrays as large as 1000 droplets. Total array vaporization rates were found to be maximized at a specific droplet number density that depends on liquid volume within the array.

From an experimental point of view, in the analysis of spray measurements it is difficult, in fact almost impossible, to separate the relative influences of the environmental and injection parameters. These problems are not encountered for linearly streaming monodisperse droplets. The size, velocity, temperature and spacing of the droplets can be adjusted separately at the injection, where as the ambient conditions can be controlled [11]. This kind of droplet stream is therefore an interesting tool for investigating droplet-to-droplet interactions. Sangiovanni and Kesten [12] were perhaps the first to investigate the effects of droplet interaction on the ignition time for droplet streams injected into a hot gas environment. They noticed that a closer spacing of the droplets enhances the strength of the heat and mass diffusion from the flame region. Sangiovanni and Labowsky [13] reported measurements of the droplet lifetime under similar conditions. They found that the classical "D2-Law" is not strictly applicable to interacting droplets due to the transient nature of that interaction. Among the experimental studies available in the literature, Virepinte et al. [14] and Castanet et al. [15] carried out experiments on periodically arranged monosized ethanol droplets placed in a laminar flame produced by the combustion of their own vapour. They used

electrostatics deviation of the droplets in order to modify the droplet spacing without changing the size and velocity of the droplets at the injection. Their results emphasize that the influence of the droplet spacing on their evaporation rate is the strongest when the distance between the droplets varies from 2 to 8 times their diameter. To account for the interactions, Castanet et al. [15] suggested a correlation based on a correction of the Sherwood and Nusselt numbers of the isolated droplet by a same factor depending only the droplet spacing. However this correlation was established in the case of combusting ethanol droplets and for a relatively narrow range of experimental conditions in term of Reynolds, Spalding and Lewis numbers. Recently, Depredurand et al. [16] performed experiments on ethanol/3-pentanone bicomponent droplets evaporating into a heated enclosure under different ambient temperatures ranging from 20°C to 360°C. Results revealed that the before-mentioned correction model fails when the Lewis number (based on the diffusivity of the fuel vapour) differs significantly from the unity. Since the droplet spacing is not sufficient to interpret these cases, the authors stressed the importance of other parameters related to the fuel nature (like its specific volatility) to describe the effect of droplet-to-droplet interactions on heat and mass transfers.

The purpose of this study is to give some insight into these effects linked to the fuel nature. To that end, six fuel compounds have been selected because of their different volatilities (acetone, ethanol, 3-pentanone, n-heptane, n-decane, n-dodecane). Monodisperse chains of droplets, streaming linearly, are injected into a temperature controlled enclosure. The size and temperature of the droplets are measured using optical techniques. Data are then processed to estimate Nusselt and Sherwood numbers with the requirement that they should fulfil the energy balance of the evaporation. Finally, the derived Nusselt and Sherwood numbers are compared to their counterparts for an isolated droplet (for which well-established models already exist) in order to quantify the effect of the droplet interactions.

## EXPERIMENTAL SET-UP

A monodisperse droplet stream is generated by disintegration of a liquid jet undergoing vibrations from a piezoceramic [11]. The liquid temperature is regulated in the injector body and the temperature is measured accurately close to the injection point with a K type thermocouple. The droplets are then injected into an enclosure fed with hot air coming from an electrical heater (figure 1). The air flowrate can be adjusted and its value is measured upstream from the heater. In order to limit the thermal losses, a resistive electrical wire is inserted within the enclosure wall so that the wall temperature can be regulated to match the one of the entering air. Temperature up to 400°C can be reached. Additionally, glass windows have been mounted in the wall to have optical accesses. Destabilization of the droplet stream by the air motion can be a critical issue in this experiment. The air velocity is therefore maintained between 0.1 m/s and 0.3 m/s and the air flow is quietened by forcing it to go through drilled wall and metallic foam. The problem of vapor saturation must be considered carefully due to the moderate air blowing and the finite dimension of the chamber which has an inner diameter of 10 cm and a height of 14 cm. An estimate of the diffusion length $L$ can be obtained considering a diffusivity $\alpha$ of $10^{-5}$ m2/s and a diffusion duration t equal to 1s. The latter corresponds to the time for a particle to be transported by the air stream through the enclosure. $L = \sqrt{\alpha t}$ is about 3 mm which is negligible compared to the inner radius of the enclosure. This insures non-statured conditions.

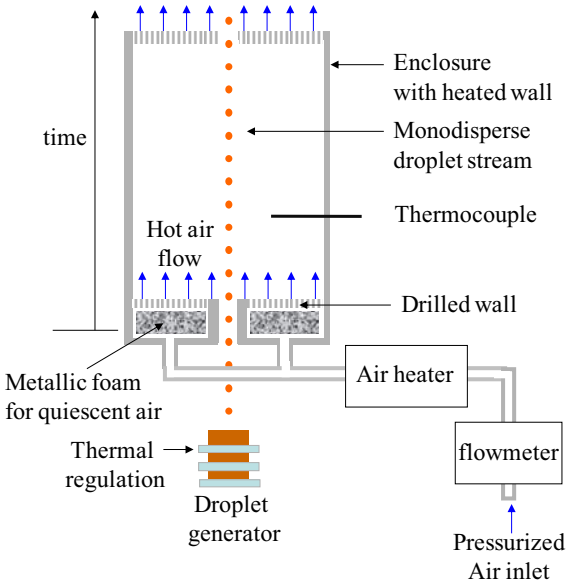


*Figure 1: Layout of the heated enclosure and the droplet generator.*

## TWO-COLOUR LASER-INDUCED FLUORESCENCE

Only an outline of the two-colour laser-induced fluorescence technique (2cLIF) is given in this section. The fuel is seeded with a low concentration (a few mg/l) of a dye used as a fluorescent temperature sensor. A comprehensive survey of the method can be found in [17,18]. The fluorescent tracer used presently is pyrromethene 597-C8, the fluorescence of which can be easily induced by the green line (514.5 nm) of the argon ion laser. The emission spectrum is broadband and extends over several hundreds of nanometres. It exhibits also a significant dependence on the temperature. A general expression of the fluorescence intensity collected over a spectral band $[\lambda_{i1};\lambda_{i2}]$, $i$ denoting the spectral band, is given by:

$$I_{f,i} = \int_{\lambda_{1,i}}^{\lambda_{2,i}} K_{opt,i}(\lambda) K_{spec,i}(\lambda) I_0 V_c C e^{\frac{\beta_i(\lambda)}{T}} d\lambda \approx K_{opt,i} K_{spec,i} I_0 V_c C e^{\frac{A_i}{T^2}+\frac{B_i}{T}} \quad (1)$$

where $K_{opt,i}$ is an optical constant taking into account the properties of the detection system (e.g. solid angle of detection and transmission of the optics), $K_{spec,i}$ is a constant depending solely on the spectroscopic properties of the fluorescent tracer in its solvent, both for the spectral band *i*. $I_0$ is the laser excitation intensity, $C$ is the molecular tracer concentration, $T$ is the absolute temperature, and $V_c$ is the volume from where the fluorescence photons are collected. This volume is the intersection between the laser beams, the droplet volume and the volume defined by the collecting optics. The factor $\beta(\lambda)$ characterizes the temperature dependence of the fluorescence intensity at the wavelength $\lambda$ [19]. $A_i$ and $B_i$ are coefficients introduced empirically to account for the temperature dependence of the fluorescence emitted over the spectral band $I$ [18]. To properly measure the

temperature of a moving and potentially evaporating droplet, the influence of the parameters $C.V_c$ and $I_0$ must be removed. The collection volume $V_c$ is constantly changing as the droplet crosses the probe volume. Furthermore, the distribution of the laser intensity within the droplet depends on the relative position of the droplet and also on the laser beam shape, which is influenced by the refractive and focusing effects at the droplet surface. To avoid these drawbacks, the fluorescence intensity is detected on two spectral bands, the temperature sensitivity of which is strongly different. The ratio of the fluorescence intensities collected on both optimized spectral bands is given by:

$$R_{12} = \frac{I_{f,1}}{I_{f,2}} = \frac{K_{opt,1}}{K_{opt,2}} \frac{K_{spec,1}}{K_{spec,2}} e^{\frac{A_1 - A_2}{T^2} + \frac{B_1 - B_2}{T}} \qquad (2)$$

This ratio is independent on the dimensions of the probe volume. The influence of the local laser intensity and the tracer concentration are eliminated as well. The position of the two detection spectral bands is optimized in order to maximize the temperature sensitivity of the fluorescence ratio $R_{12}$.The use of a single reference point where temperature is known allows eliminating the optical and spectroscopic constants $K_{opt}$ and $K_{spec}$. The excitation volume is formed by means of the beam system of a laser Doppler Anemometer (Figure 2) allowing the simultaneous measurement of the droplet velocity. This volume corresponds to an ellipsoid of revolution which is 1500 µm long in the direction of the beams and 150 µm long transversally. A volume-averaged temperature can be obtained using an excitation volume with a diameter comparable to the droplet size and by averaging the fluorescence signal over the overall transit time of the droplet in the measurement volume. The fluorescence signal is transmitted by an optical fibre to a set of beamsplitters and optical filters, which divide the fluorescence signal into the two spectral bands of interest. Mie scattering is eliminated using a highpass filter with a high optical density at the laser wavelength. The fluorescence signal is detected over the two spectral bands by means of two photomultiplier tubes equipped with two rapid preamplifiers. The technique provides the temperature with an accuracy estimated at ±1°C. An interesting feature of pyrromethene 597-C8 relates to its temperature sensitivity $\beta(\lambda)$ that is almost unchanged when dissolved into any of the selected fuels (acetone, ethanol, 3-pentanone, n-heptane, n-decane, n-dodecane). Therefore, identical spectral bands of detection [540 nm ; 560 nm] and [590 nm ; 610 nm] can be selected without detriment to the measurement accuracy.

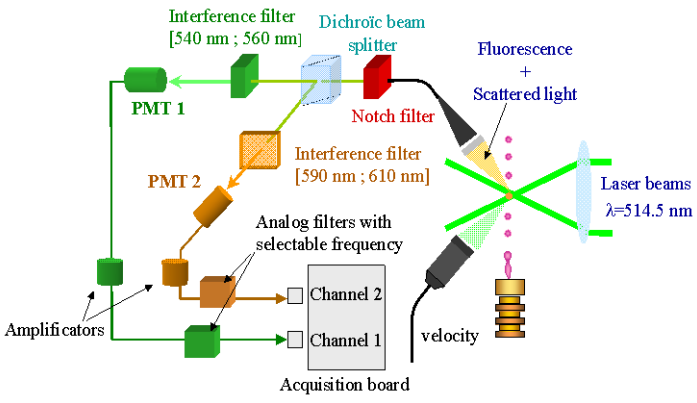


*Figure 2: 2cLIF optical set-up.*

## FORWARD SCATTERING INTERFEROMETRY (FSI)

Knowledge of the droplet size reduction is necessary to characterize the evaporation of the droplets. The measurement technique is based on the interaction between a spherical droplet and a laser beam [20]. A beam issuing from an argon ion laser is focused on a droplet (figure 3). Interferences between rays of order 0 and 1 are generated in the forward direction. The high frequency of the droplet passage makes that the fringe pattern appears stationary. Measurement of the angular interfringe near the forward scattering angle of 30° enables to determine the droplet diameter within ±0.5 µm with a very limited sensitivity to the droplet refractive index [21]. The interference pattern is focused in one direction by means of a cylindrical lens in order to increase the light power density. Image of the spatial intensity distribution is formed on the linear sensor chipset of a CCD camera (4096 pixels). The angular interfringe is measured between two interference maxima in order to derive the droplet size as suggested by Frohn and Roth [11].

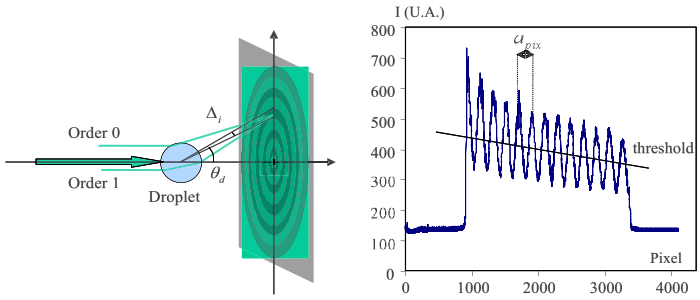


*Figure 3: Schematic view of the interference pattern in the forward scattering direction (θ: scattering angle, Δι: angular interfringe).*

The distance parameter (dimensionless spacing between the droplets) is then simply derived from the droplet size $D$ and the injection frequency $f$ by:

$$C = V/(f\,D) \qquad (3)$$

## ENERGY BALANCE OF THE EVAPORATION

The case of a moving evaporating droplet with a regressing surface is considered in this section. The radiation exchanges are neglected, which is justified by the moderate ambient temperature within the enclosure less than 400°C. Assuming that the local heat fluxes at the droplet surface are uniformly distributed, the overall energy balance of the evaporation can be summarized as followed:

$$Q_L = \Phi_C - \Phi_{vap} \qquad (4)$$

where $Q_L$ is the heat flux entering into the droplet (responsible for the droplet change in temperature $T_m$, see eq.16), $\Phi_C$ is the convective heat flux transferred from the gas and $\Phi_{vap}$ is the heat flux due to vaporization defined by:

$$\Phi_{vap} = -L_v(T_S)\dot{m} \qquad (5)$$

$\Phi_C$ and $\Phi_{vap}$ can be derived from Nusselt and Sherwood numbers defined by:

$$\Phi_c = \pi \lambda_g D Nu (T_\infty - T_S) \qquad (6)$$

$$\dot{m} = \pi \rho_g D D_g B_M Sh \qquad (7)$$

where $B_M$ is the Spalding mass transfer number defined by:



3

$$B_M = \left( \frac{Y_S - Y_{amb}}{1 - Y_S} \right) \quad (8)$$

The fuel vapour mass fraction $Y_S$ at the droplet surface is determined assuming a liquid-vapour equilibrium:

$$\chi_S = P_{sat}(T_S)/P \quad (9)$$

where $P_{sat}$ denotes the saturation pressure of the fuel and $\chi_S$ the vapour molar fraction at the droplet surface related to $Y_S$ by:

$$Y_S = \frac{\chi_s M_v}{\chi_s M_v + (1-\chi_s) M_{air}} \quad (10)$$

$M_v$ and $M_{air}$ are respectively the molar mass of the vapour and the air.

In equations 6 and 7, the gas properties $\rho_g, D_g, \lambda_g$ should be estimated at a reference state according to the '1/3 rule'[22]:

$$\begin{aligned} T_{ref} &= T_s + (T_\infty - T_s)/3 \\ Y_{ref} &= Y_S + (Y_\infty - Y_S)/3 \end{aligned} \quad (11)$$

From eqs.(4-10), it appears that the experimental characterization of the heat and mass transfers parameters, i.e. the Nusselt and Sherwood numbers, requires the determination of the time evolution of the droplet mass, the surface temperature and also the droplet mean temperature.

## DATA PROCESSING

An investigation of many droplet streams was performed. The temperature, velocity and diameter of the droplet were measured simultaneously at each measurement point. The periodicity of the droplet and its steadiness allows converting the droplet distance from the injector into time. In the following, the origin of time is fixed near the entrance of the enclosure where the measurements start. The time elapsed from this origin to the $j+1^{th}$ measurement point is calculated by the recursive relationship:

$$t_{j+1} = t_j + \frac{L_{j+1} - L_j}{(V_{j+1} + V_j)/2} \quad (12)$$

where $L_j$ is the distance of the $j^{th}$ point from the origin and $V_j$ is the velocity measured at the $j^{th}$ point. Thus, the droplet diameter and temperature evolutions can be monitored as a function of time (figures 4 and 5).

The main difficulty to find out the Nusselt and Sherwood numbers relates to the fact that the surface droplet temperature $T_S$ is not directly measured. Because of this lack, this temperature has to be estimated by a model. A step-by-step procedure has been implemented to determine the Nusselt and Sherwood numbers. As an initial guess value for the calculations, $T_S(t)$ is assumed to be equal to the volume averaged temperature of the droplet $T_m(t)$.

**Step 1:** The experimental droplet diameter is corrected from the density change due to the thermal expansion of the droplet.

$$D_{corr} = D\left(\rho(T_m)/\rho(T_{m,t=0})\right)^{1/3} \quad (13)$$

Assuming the 'D2-law', the evaporation rate $K$ is determined by the least mean square method from the expression from the experimental data according to:

$$D_{corr}^2(t) = D_{corr}^2(t=0) - K t \quad (14)$$

The mass vapour flowrate is then given by:

$$\dot{m} = -\frac{\pi}{4} \rho_l(T_{t=0}) D_{corr} K \quad (15)$$

**Step 2:** The time derivative of the temperature $dT_m/dt$ is calculated from a fitted curve interpolating the temperature measurement.

**Step 3:** Physical properties of $\rho_g, D_g, \lambda_g$ are calculated according to eq.(11).

**Step 4:** Under the same assumption than step 1, the Sherwood number is derived from eq.(7).

**Step 5:** The conservation of energy applied to a control volume corresponding to the droplet is used to evaluate $Q_L$ [15] as followed:

$$Q_L = m C_{pl} \frac{dT_m}{dt} + C_{pl}(T_S - T_m)\dot{m} \quad (16)$$

From eqs. (4-6), it is possible to determine the value of the Nusselt number.

**Step 6:** The evolutions of the droplet size and temperature are simulated using the values of Nusselt and Sherwood numbers found in step 4 and 5. To that end, the same numerical approach that has been described by Abramzon and Sirignano [2] is used, except that Nusselt and Sherwood numbers are presently known in advance. The heat diffusion equation is solved by a Crank-Nicholson scheme.

$$\frac{\partial T}{\partial t} - \frac{\xi}{R}\frac{dR}{dt}\frac{\partial T}{\partial \xi} = \frac{\alpha_{l,eff}}{R^2}\frac{\partial^2 T}{\partial \xi^2}, 0 \le \xi \le 1 \quad (17)$$

This model accounts for the convection due to internal circulation by the use of the so-called effective thermal diffusivity $\alpha_{l,eff} = \chi\, \alpha_l$ where the coefficient $\chi$ varies from about 1 (at droplet Peclet number<10) to 2.72 (at droplet Peclet number >500) [2]. For the resolution, eq.(17) is completed by eq.(4) as boundary solution and a uniform temperature is assumed for the initial condition.

**Step 7:** The evolution of the surface temperature is deduced from step 6, then calculation returns to step 3. The iterative procedure is stopped when the estimated value of Nusselt and Sherwood numbers have converged with an error less than 2%. Generally, two or three loops are required to fulfill this condition.

At any iteration, it is checked that the simulated temperature and diameter are close to the experimental measurements. This is normally insured by the interpolations in step 1 and 2.

## RESULTS AND DISCUSSION

The temperature and size of the droplets were measured for a large set of aerothermal conditions and for all the aforementioned fuel species. The ambient temperature in the enclosure was fixed at 370°C.

The evaporating behavior of the different fuels was first compared. To that end, droplet sizes and temperatures were characterized under the same conditions for all the fuels. Due to differences in atomization, the liquid pressure and temperature in the injector, as well as the piezoceramic frequency have to be adjusted from one fuel to another.

Nevertheless, as indicated in the captions of figures 4 and 5, slight differences in the initial conditions remains between the fuels. To simplify the comparison, the droplet change in temperature and the square diameter normalized by its value $D_0$ at the first measurement are displayed in the figures 4 and 5.

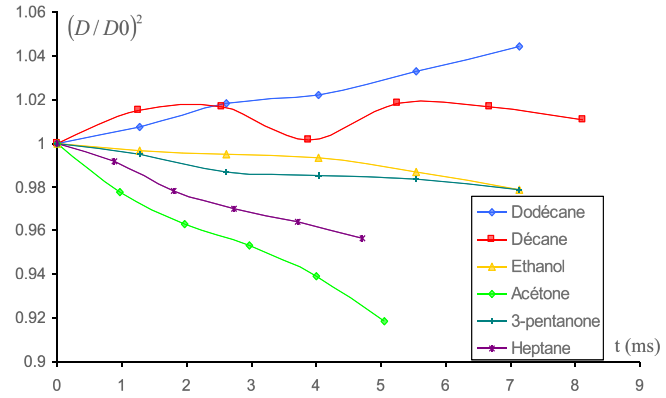


*Figure 4: Temporal evolution of the normal square diameter- $C_0$=4.5, $V_0$=9.2 (acetone:$D_0$=122.6µm, $T_0$=26.08°C ; ethanol:$D_0$=119.6µm, $T_0$=29.7°C ; heptane:$D_0$=129.3µm, $T_0$=28.6°C ; 3-pentanone:$D_0$=121.2µm, $T_0$=28.8°C ; decane:$D_0$=121.5µm, $T_0$=26.6°C ; dodecane:$D_0$=110µm, $T_0$=29.6°C).*

As expected, the evaporation rate $K$ (slope of $D^2$ as a function of time, eq.14) increases with the product volatility (figure 4). The curves range exactly in the same order than the boiling temperature of the fuels (acetone: 56.5°C, ethanol: 78.5°C, heptanes: 98.5°C, 3-pentanone: 101°C, n-decane:174°C, n-dodecane: 216°C). Significant differences can be observed among the plotted curves. In the case of decane and dodecane, evaporation is so low that it fails to compensate for the droplet expansion, especially since the heating is more important for these two fuels (figure 5). For the other fuels (acetone, ethanol, 3-pentanone, n-heptane), the square diameter follows approximately a linear trend which justifies the assumption made in the first step of the data processing.

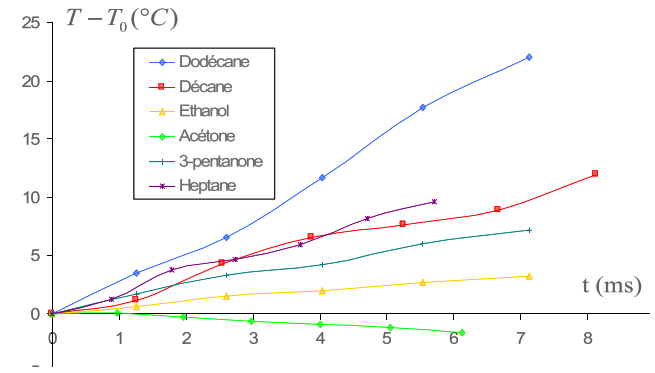


*Figure 5: Temporal evolution of the droplet variation in temperature (same conditions as figure 4).*

The droplet heating over the same period decreases with the fuel volatility (Figure 5). As stated in eq.(4), this comes from the fact that the heat flux due to vaporization $\Phi_{vap}$ is taken to the detriment of the heat flux entering into the droplet $Q_L$ which is responsible for the droplet increase in temperature. In the case of acetone, a cooling of the droplets is even observed.

The experiments have been repeated for different values of the distance parameter which is defined as the ratio between the droplet spacing and the droplet diameter (eq.3). In accordance with the data processing described before, Nusselt and Sherwood numbers have been evaluated so that the simulations (step 6) can restore accurately the droplet size and temperature evolutions while relying on a rather realistic surface temperature. Results of the simulations are presented in figures 6 and 7. They concerned only the case of n-heptane droplets.

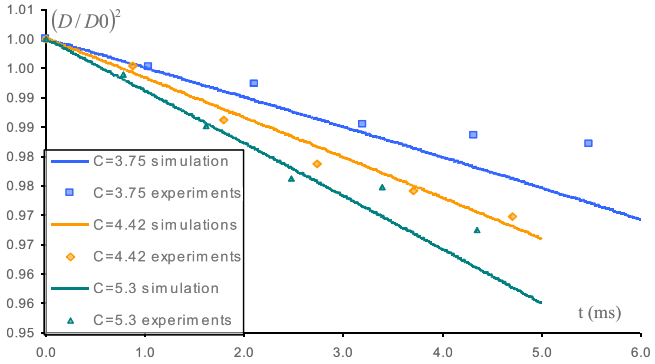


*Figure 6: Size evolution of n-heptane droplets: experiments vs simulation after adjustement of the Nusselt and Sherwood numbers (C=3.75: $D_0$=122.8µm, $V_0$=9.63m.s$^{-1}$, $T_0$=26.76°C ; C=4.42: $D_0$=131.1µm, $V_0$=11.8 m.s$^{-1}$, $T_0$=28.6°C ; C=5.3: $D_0$=134.2µm, $V_0$=14.2 m.s$^{-1}$, $T_0$=28.12°C).*

In figures 6 and 7, it can be verified that a good agreement between the experimental results and the simulations is obtained after adjustment of Nusselt and Sherwood numbers. The simulations are always included within the margin of the measurement uncertainty (about 1°C for the temperature and 1 µm for the diameter).

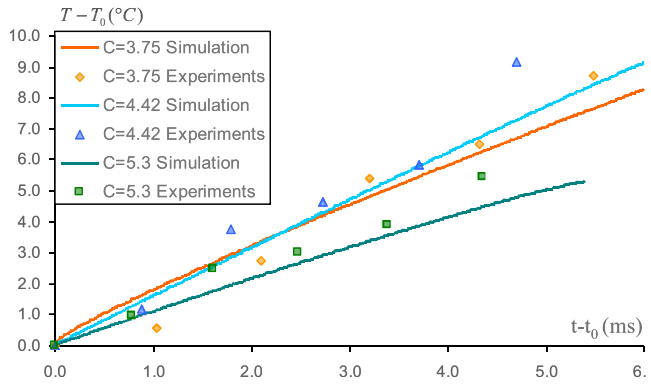


*Figure 7: Temperature evolution of ethanol droplets: experiments vs simulation after adjustement of the Nusselt and Sherwood numbers (same conditions as figure 6).*

The temporal evolution of Nusselt and Sherwood numbers are plotted in figures 8 and 9. These numbers appears to vary slowly. Additionally, a comparison between figures 8 and 9 highlights that the Sherwood number is about three time as high as the Nusselt number. This relates to differences in the value of the heat and mass diffusivities in the gaseous phase.

For an ambient temperature of 370°C, the Lewis number of the n-heptane vapour phase is about 2.25.

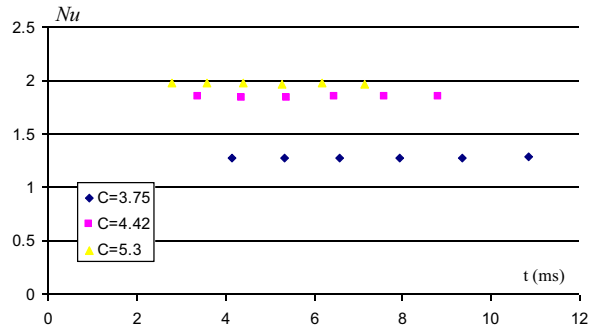


*Figure 8: Time evolution of the Nusselt number of n-heptane droplet streams (same conditions as figure 6).*

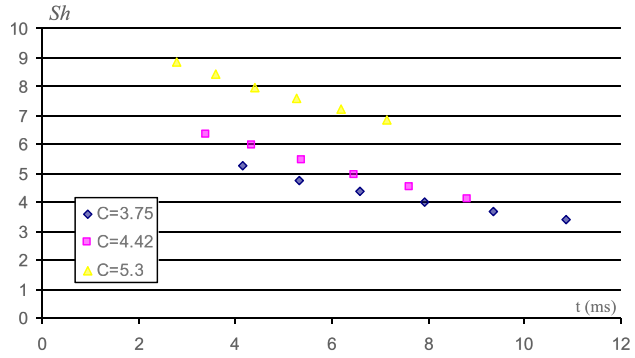


*Figure 9: Time evolution of the Sherwood number of n-heptane droplet streams (same conditions as figure 6).*

The same data processing has been implemented in the case of the other fuels. However, the evaporation being very limited in the case of decane and dodecane, it was not possible to determine the evaporation rate and thus the Sherwood number. Nevertheless, the Nusselt number of these fuels is evaluated safely by neglecting the heat flux of vaporization $\Phi_{vap}$ in the energy balance (eq.4) and by limiting the data processing to steps 2,3,5,6 and 7.

The quantification of the interaction effects on the heat and mass transfers remains difficult, since the Nusselt and Sherwood numbers depend on many parameters such as the Reynolds, Prandtl, Schmidt and Spadling numbers additionally to the distance parameter. A simple method consists in comparing the obtained values of the Nusselt and Sherwood numbers to their counterparts for an isolated droplet since theoretical models already exist and have been assessed in the case of isolated droplets. In a quasi-steady approach of the evaporation and according to the film theory [2], the expressions of the Nusselt and Sherwood numbers of an isolated evaporating moving droplet are given by:

$$Nu_{iso} = \left(\frac{\ln(1+B_T)}{B_T}\right)\left(2+\frac{Nu_0-2}{F(B_T)}\right) \qquad (18)$$

$$Sh_{iso} = \left(\frac{\ln(1+B_M)}{B_M}\right)\left(2+\frac{Sh_0-2}{F(B_M)}\right) \qquad (19)$$

$Nu_0$ and $Sh_0$ correspond to the Nusselt and Sherwood numbers without the influence of the Stefan flow. Abramzon and Sirignano [2] suggest the use of the following correlations by Clift et al. [23]:

$$Nu_0 = 1+(1+\mathrm{Re}\,\mathrm{Pr})^{1/3} f(\mathrm{Re}) \qquad (20)$$

$$Sh_0 = 1+(1+\mathrm{Re}\,Sc)^{1/3} f(\mathrm{Re}) \qquad (21)$$

with $f(\mathrm{Re}) = 1$ at $\mathrm{Re} \le 1$ and $f(\mathrm{Re}) = \mathrm{Re}^{0.077}$ at $\mathrm{Re} \le 400$.

*F(B)* is a function introduced by Abramzon and Sirignano [2] which should be applied in order to account for the effect of Stefan flow on the evaporation, since the fuel vapour flow tends to modify the convective transport around the droplet:

$$F(B) = (1+B)^{0.7}\frac{\ln(1+B)}{B} \qquad (22)$$

In eq.(18) $B_T$ denotes the heat transfer Spalding number defined as:

$$B_T = \frac{Cp_g\,(T_{amb}-T_S)}{L_v + Q_L/\dot{m}} \qquad (23)$$

The ratios $Nu/Nu_{iso}$ and $Sh/Sh_{iso}$ are depicted in figures 10 and 11 as a function of the distance parameter $C$ for all the tested conditions. The plotted values were calculated from the average value of *Nu* and *Sh* over the time interval explored in the measurements. It has been checked that the time variation of these numbers is rather limited (figures 8 and 9).

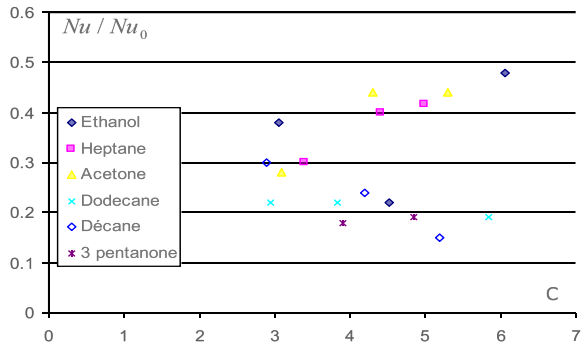


*Figure 10: Normalized Nusselt number $Nu/Nu_0$ as a function of the distance parameter.*

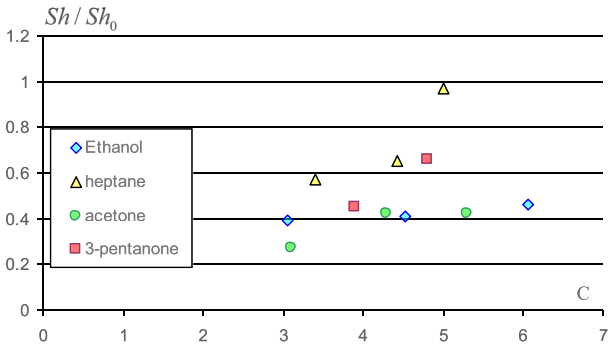


*Figure 11: Normalized Sherwood number $Sh/Sh_0$ as a function of the distance parameter.*

A relatively large dispersion of the experimental data can be observed. Nonetheless, the data can be compared to the results from Castanet et al. [15] and Atthasit et al. [24]. They studied the case of ethanol droplets in a flame [15] or in the thermal boundary layer of a heated plate. To take into account the effect of interactions, both authors suggesting a correlation depending only on the distance parameter $C$ (table 1).

For a distance parameter ranging between 3 and 6, $Nu/Nu_{iso}$ is about 0.3 in average which is significantly less than the value found by Castanet et al. [15] and Atthasit et al. [24]. However, their results were limited to the case of ethanol and were obtained at different ambient temperature. The same ratio seems to be even smaller for the less volatile fuel, i.e. n-decane and n-dodecane. In the present study, the distance

parameter $C$ does not appear to be of prime importance to describe the effects of interactions in the measurement conditions.

| | $C$=3 | $C$=4 | $C$=5 | $C$=6 |
|---|---|---|---|---|
| Castanet et al. [15] | 0.25 | 0.55 | 0.75 | 0.87 |
| Atthasit et al. [24] | 0.42 | 0.5 | 0.58 | 0.66 |

*Table 1: Correction of the effect of droplet-to-droplet interactions on the heat and mass transfers according to Castanet et al. [15] and Atthasit et al. [24].*

As a first attempt to give a model, the characteristic time of the vapour transport through the film surrounding the droplet was compared to the time period of the droplet passage. A dimensionless time $t^*$ was then formed from the ratio of these times.

$$t^* = \frac{\delta}{f V_r} \tag{24}$$

In this expression, $\delta$ denotes the film thickness as defined in the film theory [2]. It has a different value in the case of the heat and mass transfers:

$$\delta_M = D\frac{F_M}{Sh_0 - 2} \tag{25}$$

$$\delta_T = D\frac{F_T}{Nu_0 - 2} \tag{26}$$

$V_r$ is the radial velocity of the vapor around the droplet surface (Stefan flow):

$$V_r = \frac{\dot{m}}{4\pi\rho_g R^2} \tag{27}$$

The dimensionless time $t^*$ allows separating the fuels according to their volatility. Its value is the most important for the less volatile product. Indeed a low volatility corresponds to a high resistance to the transfer (high value of $\delta$) and a small vapor velocity $V_r$.

The ratios $Nu/Nu_{iso}$ and $Sh/Sh_{iso}$ are plotted in figures 12 and 13 as a function of $t^*$. In figure 12, it can be noticed that the reduction of the Nusselt number due to the interaction is increasing with $t^*$. Beyond a certain value of $t^*$, the ratio $Nu/Nu_0$ does not change very much and tends to about 0.2. Apparently, a low volatility (small velocity of the vapor expulsion) is a parameter that increases the interaction effect on the heat transfer.

In the case of the Sherwood number, no trend can be pointed from the data in figure13.

## CONCLUSION

Simultaneous measurements of the droplet size and mean temperature evolutions allowed evaluating the Nusselt and Sherwood numbers. One difficulty comes from the lack of knowledge about the droplet surface temperature. This temperature is central since it controls the vapor fraction at the droplet surface and thus the vapour flowrate. To overcome this problem, a data processing procedure has been implemented. Nusselt and Sherwood numbers as well as the droplet surface temperature are found iteratively from the comparison between simulation and experimental data.

The influence of the droplet-to-droplet interaction on the Nusselt and Sherwood numbers has been clearly quantified for fuels exhibiting very different volatilities. It appears that the Nusselt number is particularly reduced by the interactions compared to previous studies. This reduction seems to be correlated to the volatility of the fuel. An attempt to model this effect has been presented but further investigations are still required to assess the relevance of this description.

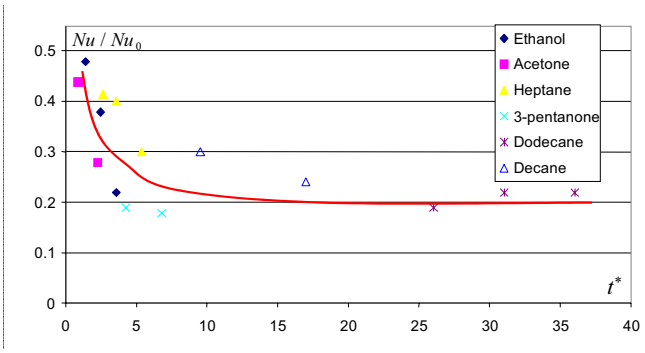


*Figure 12: Normalized Nusselt number $Nu/Nu_0$ as a function of $t^*$*

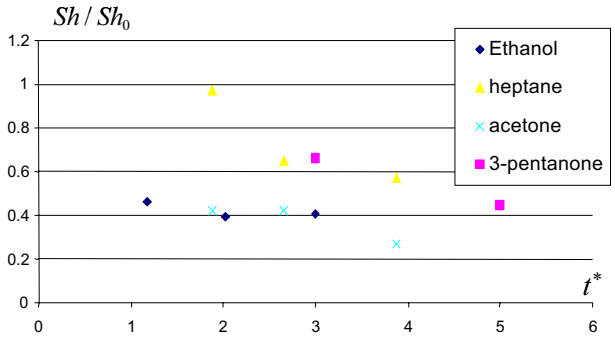


*Figure 13: Normalized Sherwood number $Sh/Sh_0$ as a function of $t^*$*


## ACKNOWLEDGMENT

This study has been conducted in the framework of the ASTRA program, supported by CNRS and ONERA.


## NOMENCLATURE

| Symbol | Quantity | SI Unit |
|---|---|---|
| $a$ | Thermal diffusity | $m^2/s$ |
| $B_M$ | Mass transfer Spalding number | |
| $B_T$ | Thermal transfer Spalding number | |
| $C$ | Distance parameter | |
| $C_0$ | Tracer concentration | mol/L |
| $C_p$ | Specific heat | J/Kg/K |
| $D$ | Droplet diameter | m |
| $D_g$ | Molecular diffusivity of the vapor | $m^2/s$ |
| $f$ | Frequency of the droplets | $s^{-1}$ |
| $I$ | Ligth intensity | $W/m^2$ |
| $K$ | A constant or the evaporation rate | $m^2/s$ |
| $Le$ | Lewis number | |
| $L_v$ | Latent heat of vaporization | J/Kg |
| m | Droplet mass | Kg |
| $\dot{m}$ | Fuel vapor flowrate | Kg/s |
| $Nu$ | Nusselt number | |
| $Pr$ | Prandtl number | |
| $Q_L$ | Heat flux entering into the droplet | W |
| $P$ | Pressure | Pa |
| $R$ | Droplet radius | M |
| $Re$ | Droplet Reynolds number | |
| $Sh$ | Sherwood number | |

| | | |
|---|---|---|
| $Sc$ | Schmidt number | |
| $T$ | Temperature | K |
| $t$ | Time | s |
| $V$ | Droplet velocity | m/s |
| $Y$ | Fuel vapor mass fraction | |

**Greek symbols**

| | | |
|---|---|---|
| $\Phi_C$ | Convective heat flux | W |
| $\Phi_{vap}$ | Vaporization heat flux | W |
| $\lambda$ | Thermal conductivity | |
| $\mu$ | Dynamic viscosity | |
| $\rho$ | Specific density | |

**Subscripts**

| | |
|---|---|
| $g$ | Gas phase |
| $L$ | Fuel liquid phase |
| $ref$ | Reference state |
| $S$ | Surface condition |
| $0$ | First point of measurement just after the entrance in the enclosure or isolated droplet |
| $\infty$ | Conditions far away from the flame front in quiescent |

**REFERENCES**


[1] W. A. Sirignano, Fluid dynamics and transport of droplets and sprays, Cambridge University Press, 1999.

[2] B. Abramzon, W. A. Sirignano, Droplet vaporization model for spray combustion calculations, International Journal of Heat and Mass Transfer 32 (1989) 1605.

[3] E.E. Michaelides, Hydrodynamic force and heat/mass transfer from particles, bubbles, and drops - the Freeman scholar lecture. ASME J Fluid Engineering 125 (2003) 209-238.

[4] S.S. Sazhin, Advanced models of fuel droplet heating and evaporation, Progress in Energy and Combustion Science 32 (2006) 162-214.

[5] M. Labowsky, Calculation of the burning rates of interacting fuel droplets, Combust. Sci. Technol. 22 (1980) 217-226.

[6] M. Marberry, A.K. Ray, K. Leung, Effect of multiple particle interactions on burning droplets, Combust. Flame 57 (1984) 237-245.

[7] C. H. Chiang, W. A. Sirignano, Interacting, convecting, vaporizing fuel droplets with variable properties, International Journal of Heat and Mass Transfer 36 (1993) 875.

[8] C. H. Chiang, W. A. Sirignano, Axisymmetric calculations of three droplet interactions, Atomization and Sprays 3 (1993) 91.

[9] R. T. Imaoka, W. A. Sirignano, Vaporization and combustion in three-dimensional droplet arrays, Proceedings of the Combustion Institute 30 (2005) 1981.

[10] R. T. Imaoka, W. A. Sirignano, Transient vaporization and burning in dense droplet arrays, Int. J. Heat Mass Transfer 48 (2005) 4354.

[11] A. Frohn, N. Roth, Dynamics of Droplets, Springer-Verlag Berlin and Heidelberg GmbH, 2000.

[12] J.J. Sangiovanni, A.S. Kesten, Effect of droplet interaction on ignition in monodispersed droplet streams, Sixteenth International Symposium on Combustion, The Combustion Institute (1976).

[13] J.J. Sangiovanni, M. Labowski, Burning times of linear fuel droplet arrays: a comparison of experiment and theory, Combust. Flame 45 (1982) 15-30.

[14] J. F. Virepinte, Y. Biscos, G. Lavergne, P. Magre, G. Collin, A rectilinear droplet stream in combustion : droplet and gas phase properties, Combustion science and technology 150 (2000) 143.

[15] G. Castanet, M. Lebouché, F. Lemoine, Heat and mass transfer of combusting monodisperse droplets in a linear stream, Int. J. Heat Mass Transfer 48 (2005) 3261.

[16] V. Deprédurand, C. Maqua, G. Castanet, F. Lemoine, Temperature measurement of evaporating ethanol/3-pentanone bicomponent droplets using 2-colour LIF, Institute for Liquid Atomization and Spray Systems, Mugla, Turkey, 2007

[17] P. Lavieille, F. Lemoine, M. Lebouché, Investigation on temperature of evaporating droplets in a linear stream using two color laser induced fluorescence, Combust. Sci. Technol. 174 (2002) 117-142.

[18] Castanet G., Lavieille P., Lebouché M., Lemoine F. (2003) Measurement of the temperature distribution within monodisperse combusting droplets in linear stream using two colors laserinduced fluorescence. Exp Fluids 35:563–571.

[19] P. Lavieille, F. Lemoine, G. Lavergne, M. Lebouché, Evaporating and combusting droplet temperature measurements using two color laser induced fluorescence, Exp. Fluids 31 (2001) 45.

[20] Koenig G.; Anders K.; Frohn A. (1986) A new light scattering technique to measure droplet diameter of periodically generated moving droplets, J. Aerosol Sci. 17: 157-167.

[21] Massoli P. (1998) Rainbow refractometry applied to radially inhomogeneous spheres : the critical case of evaporating droplets, Applied Optics 37: 3227-3235.

[22] G. L. Hubbard, V. E. Denny, A. F. Mills, Droplet evaporation: effects of transients and variable properties, International Journal of Heat and Mass Transfer. 18 (1975) 1003.

[23] R.Clift,J.R. Grace and M.E. Weber, Bubbles, Drops and Particles, Academic Press, New York (1978).

[24] Atthasit A, Doué N, Biscos Y, Lavergne G. Influence of droplet concentration on the dynamics and evaporation of a monodisperse stream of droplets in evaporation regime. In: First international symposium on combustion and atmospheric pollution, St-Petersburg, Russia, July 8–11; 2003.